Capture Deformation Twinning in Mg during Shock Compression with Ultrafast Synchrotron X-Ray Diffraction

S. Chen, Y. X. Li, N. B. Zhang, J. W. Huang, H. M. Hou, S. J. Ye, T. Zhong, X. L. Zeng, D. Fan,
L. Lu, L. Wang, T. Sun, K. Fezzaa, Y. Y. Zhang, M. X. Tang, and S. N. Luo

Capture deformation twinning in Mg during shock compression with ultrafast synchrotron X-ray diffraction

S. Chen,[1] Y. X. Li,[1] N. B. Zhang,[1] J. W. Huang,[1] H. M. Hou,[2] S. J. Ye,[1] T. Zhong,[1] X. L. Zeng,[1] D. Fan,[1] L. Lu,[2] L. Wang,[3] T. Sun,[4] K. Fezzaa,[4] Y. Y. Zhang,[1, *] M. X. Tang,[1, †] and S. N. Luo[1, 2, ‡]

[1] *The Peac Institute of Multiscale Sciences, Chengdu, Sichuan 610031, P. R. China*
[2] *Key Laboratory of Advanced Technologies of Materials, Ministry of Education, and Institute of Materials Dynamics, Southwest Jiaotong University, Chengdu, Sichuan 610031, P. R. China*
[3] *College of Science, Hunan Agricultural University, Changsha, Hunan 410128, P. R. China*
[4] *Advanced Photon Source, Argonne National Laboratory, Argonne, Illinois 60439, USA*
(Dated: December 2, 2019)

Deformation twinning plays a vital role in accommodating plastic deformation of hexagonal close-packed (HCP) metals, but its mechanisms are still unsettled under high strain rate shock compression. Here we investigate deformation twinning in shock-compressed Mg as a typical HCP metal with *in situ*, ultrafast synchrotron X-ray diffraction. Extension twinning occurs upon shock compression along $\langle 11\bar{2}0 \rangle$ and $\langle 10\bar{1}0 \rangle$, but only upon release for loading along $\langle 0001 \rangle$. Such deformation mechanisms are a result of the polarity of deformation twinning which depends on directionality and relative magnitude of resolved shear stress, and may be common for Mg and its alloys in a wide range of strain rates.

Mg and its alloys represent the lightest metal class with a remarkable potential in engineering applications for their high specific stiffness and high specific strength [1–7]. Nonetheless, a wide application of Mg and its alloys is hindered by their poor ductility [1, 2, 8–10], and overcoming such a deficiency requires a full understanding of deformation mechanisms under various service conditions across a wide range of strain rates [11–16], including high strain rate impact loading. In hexagonal close-packed (HCP) metals, deformation twinning plays an exceptionally important role in accommodating plastic deformation given their limited slip systems compared to face-centered cubic metals [17–19]. It is also highly desirable to investigate Mg as a typical HCP metal for understanding deformation twinning in HCP metals in general.

In situ synchrotron-based transient X-ray diffraction (TXD) measurements reveal a strong anisotropy in deformation of rolled Mg alloys under quasi-static [11] and medium strain rate split Hopkinson pressure bar [12] compression: pronounced extension twinning occurs for loading axis (LA) perpendicular to the *c*-axis, while dislocation slip prevails for LA parallel to the *c*-axis. Such deformation mechanisms are common for both low and medium strain rate compression under one-dimensional (1D) stress condition [11, 12].

At even higher stain rates, e.g., upon plate-impact shock compression, elevated strain rate and temperature, as well as more complex stress condition (1D strain), may lead to different dislocation-twinning mechanisms. Deformation twins were observed in shocked single crystal Mg via postmortem examination. However, a recent TXD study [13] on single crystal Mg suggests that deformation twins in a postmortem sample may have formed upon release rather on shock compression. It remains inconclusive regarding deformation mechanisms of Mg under high strain rate shock compression, since TXD experiments only explored loading along $\langle 0001 \rangle$ or the *c*-axis, while postmortem microstructure can be different from that at the corresponding shock-compression state. It is well known that plastic deformation is rate-dependent and may also depend on stress states (1D stress vs. 1D strain). Two outstanding questions still remain: what deformation mechanisms in Mg under high strain rate shock compression, in particular, deformation twinning, and whether the mechanisms are common regardless of strain rate and stress state.

Here, we use a recently developed technique [20, 21], *in situ* ultrafast synchrotron TXD with sub-ns exposure time, to probe shock-compressed single-crystal magnesium, and reveal its lattice-scale deformation mechanisms under dynamic compression, in particular for deformation twinning. We report on the first direct observation of deformation twinning during planar shock wave compression of Mg single crystals along different orientations. Deformation twinning of magnesium, a typical HCP metal, is strongly orientation dependent during shock compression: extension twinning occurs for loading along $\langle 10\bar{1}0 \rangle$ and $\langle 11\bar{2}0 \rangle$, while twinning is absent for $\langle 0001 \rangle$. Shear deformation analysis and molecular dynamics simulations reveal that such an anisotropy is governed by the directionality [22, 23] and magnitude of resolved shear stress.

Plate impact experiments coupled with *in situ* ultrafast Laue diffraction measurements on single-crystal Mg are performed at beamline 32-ID-B of the Advanced Photon Source (APS; Fig. 1). A "pink" X-ray beam from an undulator insertion device is used for Laue diffraction measurements (Fig. S1 in Supplementary Information, SI [24]). Shock-compression is achieved via impact by a flat-faced polycarbonate projectile launched with a two-stage gas gun. The exposure time for the diffraction cameras is about 80 ps (single bunch). Two diffraction patterns are
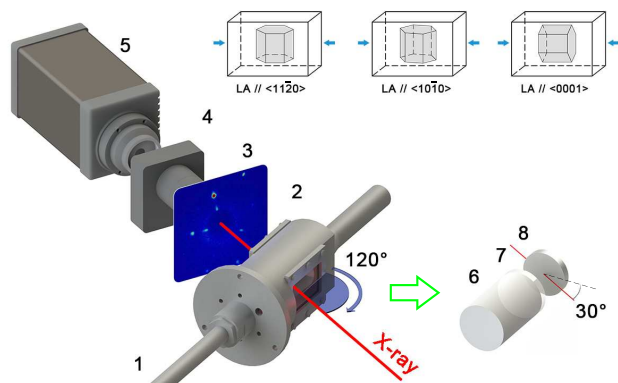
FIG. 1. Schematic of gas-gun loading and sub-ns X-ray diffraction measurements. 1: gun barrel; 2: sample chamber; 3: scintillator; 4: image intensifier; 5: gated camera(s); 6: polycarbonate sabot; 7: polycarbonate flyer plate; 8: single-crystal Mg sample. Top right: orientation relations between impact loading axis (LA) and crystallographic orientation of single-crystal Mg sample.

FIG. 2. Shock compression along $\langle 11\bar{2}0 \rangle$. (a) Measured diffraction pattern 335 ns before impact. (b) Measured diffraction pattern 124 ns after impact showing twinning spots. (c) Simulated diffraction pattern corresponding to (b). The matching font colors of Miller indices refer to ambient (white) and twinning (orange) spots. (d) Schematic showing extension twinning mechanisms for loading along $\langle 11\bar{2}0 \rangle$.

recorded for each shot, one before impact and the other, during shock compression or release. Free surface velocity history is measured with a Doppler pin system, and used to monitor the evolution of elastic and plastic shock waves; the states of a compressed sample probed by simultaneous TXD can be determined accordingly. The combination of ultrafast synchrotron TXD and gas gun loading allows us to examine instantaneous deformation mechanisms of single crystal Mg during shock compression with sub-nanosecond time resolution.

Mg single crystals are shock-loaded along three typical crystallographic orientations, $\langle 0001 \rangle$, $\langle 10\bar{1}0 \rangle$ and $\langle 11\bar{2}0 \rangle$. Details about the Mg samples, TXD experiments, and data analysis are presented in SI [24]. A total of six TXD experiments are conducted at different impact velocities, and TXD probes different states of shock compression or subsequent release. The experimental parameters are listed in Table S1 of SI [24]. Deformation twinning is observed from dynamic diffraction patterns for loading directions perpendicular to the c-axis, i.e., $\langle 10\bar{1}0 \rangle$ and $\langle 11\bar{2}0 \rangle$, but not for loading directions parallel to the c-axis, i.e., $\langle 0001 \rangle$. We present below some diffraction patterns for shock compression along $\langle 11\bar{2}0 \rangle$ and $\langle 10\bar{1}0 \rangle$, and more results are included in SI [24].

The TXD patterns for shock loading along $\langle 11\bar{2}0 \rangle$ are shown in Fig. 2. The exact sample orientation right before impact is obtained via indexing the corresponding diffraction pattern [Fig. 2(a)] [25]. Upon shock compression, intensity/position of an original Laue spot may change along with the appearance of new diffraction spots [Fig. 2(b)]. The latter represents crystallographic orientation changes within the parent sample matrix associated with deformation twinning. To find the relationship between original and twinning spots, we conduct
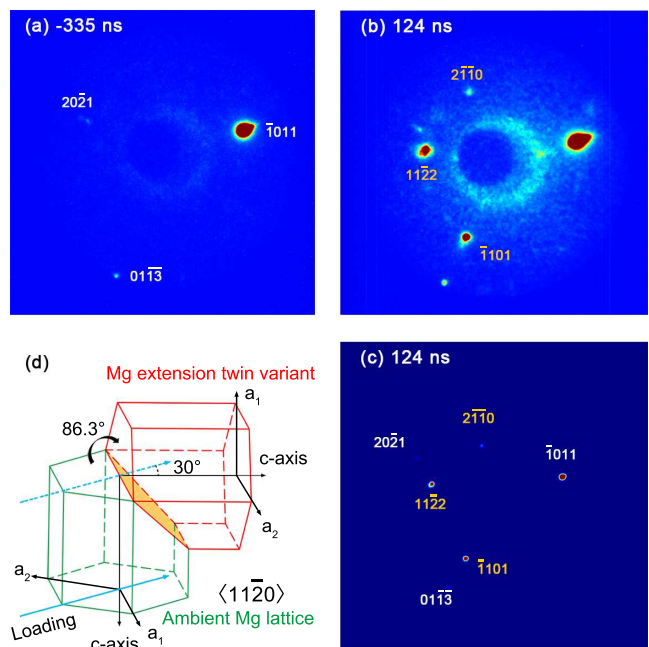
Laue X-ray diffraction simulations for all possible contraction and extension twinning scenarios in Mg (Fig. S4 in SI [24]), and compare them with the experimental patterns, considering both the position and relative intensity of a diffraction spot. The best-match twinning crystals can be found for a dynamic diffraction pattern [Fig. 2(c)], and the match in position and relative intensity between the predicted pattern based on the twinning and the measured TXD pattern [Fig. 2(b)] is excellent. The new diffraction spots can be assigned uniquely to extension twins, and $(01\bar{1}2)[0\bar{1}11]$ is the predominant twinning system. Meanwhile, no contraction twins are identified. Fig. 2(d) shows schematically the original Mg lattice in green and extension twinning lattice in red, and their orientations relative to the shock loading direction. The angle between two {0001} planes of the original and twinning lattices is about 86.3°, characteristic of extension twinning. After twinning deformation, the c-axis of the newly formed twinning lattice is about 30° with respect to the loading direction. (More details are presented in Fig. S11 of SI.)

For loading along $\langle 10\bar{1}0 \rangle$, the diffraction patterns prior to and during shock compression are shown in Fig. 3(a) and 3(b), respectively, as well as the indices of original and new Laue spots, in Fig. 3(c). Similar to shock compression along $\langle 11\bar{2}0 \rangle$, the new diffraction spots are also due to extension twins, and the predominant twinning
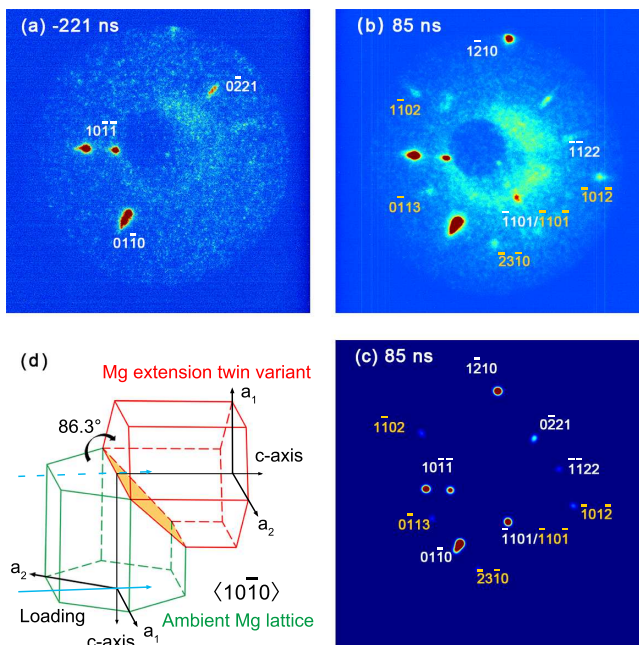
FIG. 3. Shock compression along $\langle 10\bar{1}0 \rangle$. (a) Measured diffraction pattern 221 ns before impact. (b) Measured diffraction pattern 85 ns after impact showing twinning spots. (c) Simulated diffraction pattern corresponding to (b). The matching font colors of Miller indices refer to ambient (white) and twinning (orange) spots. (d) Schematic showing extension twinning mechanisms for loading along $\langle 10\bar{1}0 \rangle$.

FIG. 4. Possible extension twinning systems for loading along (a) $\langle 11\bar{2}0 \rangle$ and (b) $\langle 10\bar{1}0 \rangle$. Colored and dotted planes are symmetrical with respect to loading direction (red arrows). Only Group II twinning systems are activated for both loading directions. See Fig. S6 for complete equivalent twinning systems.

system is $(01\bar{1}2)[0\bar{1}11]$ (no contraction twins, either). The ambient and compression-induced new lattice, and their orientation relationships with respect to the loading direction, are shown in Fig. 3(d). The c-axis of the twinning variant is nearly parallel ($\sim 4°$) to the loading direction.

For shock loading along $\langle 0001 \rangle$ or the c-axis (Fig. S8 in SI [24]), no twinning diffraction spots are observed during shock compression at different impact velocities (up to 2081 m/s; Fig. S9 and Fig. S10 in SI [24]). However, new diffraction spots emerge upon release (Fig. S8 in SI [24]), and can be attributed to extension twinning as well. The absence of deformation twinning upon shock compression and its appearance upon release are consistent previous experiments [13].

The ultrafast TXD measurements reveal that extension twinning is the predominate deformation mechanism for compression loading along $\langle 11\bar{2}0 \rangle$ and $\langle 10\bar{1}0 \rangle$ (perpendicular to the c-axis), as well as upon release for loading along $\langle 0001 \rangle$ or the c-axis, although deformation twinning is absent upon shock compression along the c-axis. As shown below, the anisotropy of deformation twinning, either upon shock compression or release, can be explained in terms of resolved shear stress (direction and amplitude) and unidirectionality (polarity) [22, 23] of deformation twinning in HCP metals.

The principal twinning systems of Mg are shown in Fig. 4 and Fig. S6 in SI [24]. For HCP metals like Mg,

there are six twinning planes crystallographically symmetric around the c-axis, or six variants each for extension or contraction twinning. For single crystals under shock compression (1D-strain condition), the symmetry can be broken, and resolved shear stress (RSS) and activated twinning planes are inevitably associated with loading direction. In addition, since stress state is much more complicated in 1D-strain loading than that in conventional 1D-stress loading, full stress tensors should be considered for the RSS analysis of shock compression.

For deformation twinning, let $\tilde{\eta}_1$ be the unit direction vector along twinning direction, and $\tilde{\tau}$, the RSS vector. The polarity of deformation twinning in HCP metals requires that $\tilde{\eta}_1$ and $\tilde{\tau}$ be of the same direction, i.e.,

$$\tilde{\eta}_1 \cdot \tilde{\tau} > 0. \qquad (1)$$

We thus calculate $\tilde{\eta}_1 \cdot \tilde{\tau}$ normalized by $|\sigma_{xx}|$ for different twinning systems in Mg shock-compressed along different directions (Tables S2–S4 in SI [24]). Here σ_{xx} is shock stress. Twinning is more likely to occur for larger positive $\tilde{\eta}_1 \cdot \tilde{\tau}/|\sigma_{xx}|$ values. For shock compression along $\langle 11\bar{2}0 \rangle$ and $\langle 10\bar{1}0 \rangle$, $\tilde{\eta}_1 \cdot \tilde{\tau}/|\sigma_{xx}|$ is positive for extension twinning and negative for contraction twinning, so only extension twinning is allowed. For loading along $\langle 0001 \rangle$, $\tilde{\eta}_1 \cdot \tilde{\tau}/|\sigma_{xx}|$ is negative for extension twinning and positive for contraction twinning, and thus, extension twinning is prohibited upon compression. However, the critical resolved

shear stress for dislocation slip is much lower than that for contraction twinning (45–81 MPa for $\langle c + a \rangle$ pyramidal slip and 76–153 MPa for contraction twinning) [26], so dislocation slip dominates over contraction twinning under shock compression along $\langle 0001 \rangle$. On the other hand, RSS reverses its sign upon release (reducing compression is equivalent to tension), so extension twins are activated as seen in the experiments.

For shock compression along $\langle 11\bar{2}0 \rangle$, the extension twinning planes are divided into two groups [Fig. 4(a), and Fig. S6 in SI]. For Group I, loading direction is parallel to the twinning planes and RSS is nearly zero, so such twinning systems can not be activated. Group II twinning systems are more likely to be activated given their highest RSS (Table S2). In Group II, there are four equivalent extension twinning planes with respect to loading direction [only two of them are shown in Fig. 4(a)], and the twinning planes are at a finite angle with the loading direction. In experiments, there exist small deviations of $1° − 3°$ from the nominal sample orientation, which may render extension twinning system $(01\bar{1}2)[0\bar{1}11]$ (A_2 in Group II) become the predominant twinning system, giving rise to the only observed diffraction pattern in Fig. 2(b), as a result of symmetry loss induced by this misorientation.

For shock compression along $\langle 10\bar{1}0 \rangle$, the twinning planes in Groups I and II are at different angles with the loading direction; there are four equivalent extension twinning planes in Group I [only two are shown in Fig. 4(b)] and two in Group II. RSS in Group II is much higher than that on Group I (Table S3 in SI). Extension twinning system $(01\bar{1}2)[0\bar{1}11]$ (B_2 in Group II) should be the predominant deformation twinning mechanism based on the directionality and magnitude of RSS, as observed in the experiments.

When shock-compressed along $\langle 0001 \rangle$ or the c-axis, extension twinning can not be activated due to the polarity of deformation twinning in HCP metals (Fig. S7 in SI). However, dislocation slip does not have polarity and can be activated. Although contraction twinning is not prohibited, its critical resolved shear stress is higher than that for pyramidal slip [13, 26, 27]. As a result, pyramidal slip becomes the dominant deformation mechanism during shock compression. Extension twinning system $\{10\bar{1}2\}\langle\bar{1}011\rangle$ is activated since RSS reverses its direction upon release, and RSS is larger and critical resolved shear stress is lower than pyramidal slip [27–29].

Given the twinning mechanisms as revealed from the above RSS analysis, we simulate TXD patterns and compare them with the measurements, and excellent agreement is found, confirming the extension twinning systems identified from the RSS analysis. In addition, our MD simulations show similar deformation twinning behaviors and deformation mechanisms as observed in the experiments (Fig. S5 in SI).

The TXD measurements and diffraction analysis, re-solved shear stress analysis, and MD simulations elucidate the dislocation-twinning deformation mechanisms in Mg under shock loading. The TXD results presented here are similar to those of medium and low strain rates loading on Mg alloys, such as quasi-static and Hopkinson bar loading [11, 12], and the underlying mechanisms of deformation twinning are likely common across a wide range of strain rate.

The *in situ*, real time, ultrafast Laue X-ray diffraction measurements have captured deformation twinning in single-crystal Mg of different orientations upon shock compression or upon release. Deformation twinning is anisotropic. Extension twinning occurs upon shock compression along along $\langle 11\bar{2}0 \rangle$ and $\langle 10\bar{1}0 \rangle$, but only upon release for loading along $\langle 0001 \rangle$. Such deformation twinning is a result of its polarity, depending on directionality and relative magnitude of RSS. These high strain rate 1D-strain experiments along with previous *in situ* diffraction experiments under lower strain rate 1D-stress loading on Mg alloys, appear to point to the common mechanisms for deformation twinning in Mg and its alloys, and likely in HCP metals in general.

* yyzhang@pims.ac.cn
† mxtang@pims.ac.cn
‡ sluo@pims.ac.cn

[1] Z. X. Wu, R. Ahmad, B. L. Yin, S. Sandlöbes, and W. Curtin, Science **359**, 447 (2018).
[2] B. Y. Liu, F. Liu, N. Yang, X. B. Zhai, L. Zhang, Y. Yang, B. Li, J. Li, E. Ma, J. F. Nie, et al., Science **365**, 73 (2019).
[3] M. Lentz, M. Risse, N. Schaefer, W. Reimers, and I. J. Beyerlein, Nat. Commun. **7**, 11068 (2016).
[4] T. M. Pollock, Science **328**, 986 (2010).
[5] L. Y. Chen, J. Q. Xu, H. Choi, M. Pozuelo, X. long Ma, S. Bhowmick, J. M. Yang, S. Mathaudhu, and X. C. Li, Nature **528**, 539 (2015).
[6] B. Li and E. Ma, Phys. Rev. Lett. **103**, 035503 (2009).
[7] Z. Zeng, J. F. Nie, S. W. Xu, C. H. J. Davies, and N. Birbilis, Nat. Commun. **8**, 972 (2017).
[8] Q. Yu, J. Wang, Y. Jiang, R. J. McCabe, N. Li, and C. N. Tomé, Acta Mater. **77**, 28 (2014).
[9] R. H. Taylor, S. Curtarolo, and G. L. W. Hart, Phys. Rev. B **84**, 084101 (2011).
[10] M. Uranagase and R. Matsumoto, Phys. Rev. B **89**, 224103 (2014).

[11] L. Lu, J. W. Huang, D. Fan, B. X. Bie, T. Sun, K. Fezzaa, X. L. Gong, and S. N. Luo, Acta Mater. **120**, 86 (2016).

[12] L. Lu, T. Sun, K. F. K, X. L. Gong, and S. N. Luo, Mater. Sci. Eng. A **701**, 143 (2017).

[13] S. J. Turneaure, P. Renganathan, J. M. Winey, and Y. M. Gupta, Phys. Rev. Lett. **120**, 265503 (2018).

[14] P. J. Hazell, G. J. A. Thomas, E. Wielewski, C. Stennett, and C. Siviour, Acta Mater. **60**, 6042 (2012).

[15] G. I. Kanel, G. V. Garkushin, A. S. Savinykh, S. V. Razorenov, T. D. Resseguier, W. G. Proud, and M. R. Tyutin, J. Appl. Phys. **116**, 143504 (2014).

[16] F. Zhang, M. Hao, F. C. Wang, C. W. Tan, X. D. Yu, H. L. Ma, and H. N. Cai, Scr. Mater. **67**, 951 (2012).

[17] M. Itakura, H. Kaburaki, M. Yamaguchi, and T. Tsuru, Phys. Rev. Lett. **116**, 225501 (2016).

[18] H. Q. Sun, Y. N. Shi, M. X. Zhang, and K. Lu, Acta Mater. **55**, 975 (2007).

[19] S. G. Hong, S. H. Park, and C. S. Lee, Acta Mater. **58**, 5873 (2010).

[20] S. N. Luo, B. J. Jenson, D. E. Hooks, K. Fezzaa, K. J. Ramos, J. D. Yeager, K. Kwiatkowski, and T. Shimada, Rev. Sci. Instrum. **83**, 073903 (2012).

[21] D. Fan, J. W. Huang, X. L. Zeng, Y. Li, J. C. E, J. Y. Huang, T. Sun, K. Fezzaa, Z. Wang, and S. N. Luo, Rev. Sci. Instrum. **87**, 053903 (2016).

[22] R. Glüge, *Elastic modelling of deformation twinning on the microscale* (Otto von Guericke University Library, Magdeburg, Germany, 2009).

[23] J. Čapek, M. Knapek, P. Minárik, J. Dittrich, and K. Máthis, Metals **8**, 644 (2018).

[24] See supplementary information of this article, which includes Refs. [30-35]. url : `http://test/`.

[25] V. K. Gupta and S. R. Agnew, J. Appl. Crystallogr. **42**, 116 (2009).

[26] J. Zhang and S. P. Joshi, J. Mech. Phys. Solids **60**, 945 (2012).

[27] B. L. Wu, Y. H. Zhao, X. H. Du, Y. D. Zhang, F. Wagner, and C. Esling, Mater. Sci. Eng. A **527**, 4334 (2010).

[28] J. J. Jonas, S. Mu, T. Al-Samman, G. Gottstein, L. Jiang, and Ė. Martin, Acta Mater. **59**, 2046 (2011).

[29] Q. Ma, H. E. Kadiri, A. L. Oppedal, J. C. Baird, B. Li, M. F. Horstemeyer, and S. C. Vogel, Int. J. Plast. **29**, 60 (2012).

[30] M. Sánchez del Río and R. J. Dejus, Proc. SPIE **5536**, 171 (2004).

[31] K. Chen and K. P. Boyle, Metallurgical and Materials Transactions A **40**, 2751 (2009).

[32] T. J. Ahrens, H. Tan, and J. D. Bass, International Journal of High Pressure Research **2**, 145 (1990).

[33] E. R. Naimon, Phys. Rev. B **4**, 4291 (1971).

[34] S. Plimpton, J. Comp. Phys. **117**, 1 (1995), also see `http://lammps.sandia.gov`.

[35] X. Y. Liu, J. B. Adams, F. Ercolessi, and J. A. Moriarty, Modell. Simul. Mater. Sci. Eng. **4**, 293 (1996).